Coulomb forces in THz electromechanical meta-atoms

Allegra Calabrese, Djamal Gacemi, Mathieu Jeannin, Stéphan Suffit, Angela Vasanelli, Carlo Sirtori, Yanko Todorov

Research article

Allegra Calabrese*, Djamal Gacemi, Mathieu Jeannin, Stéphan Suffit, Angela Vasanelli, Carlo Sirtori and Yanko Todorov*

Coulomb forces in THz electromechanical meta-atoms

https://doi.org/10.1515/nanoph-2019-0314
Received August 12, 2019; revised October 1, 2019; accepted October 1, 2019

Abstract: Thanks to their large sensitivity to electromagnetic fields, microelectromechanical systems are becoming attractive for applications in the THz band (0.1–10 THz). However, up to date all THz electromechanical systems couple electromagnetic fields to mechanical motion only through photothermal dissipative forces: such mechanism allows for sensitive detection but prevents applications that require coherent transfer of information. In this work, we present a THz electromechanical meta-atom where the coupling between an electromagnetic mode and the displacement of a metallic micro-beam is substantially controlled by a conservative Coulomb force due to charge oscillations in the nanometric-size capacitive part of the meta-atom. We present experiments, performed at room temperature, which allow distinguishing and precisely quantifying the contributions of conservative and dissipative forces in the operation of our electromechanical resonator. Our analysis shows that the Coulomb force becomes the dominant contribution of the total driving force for high-order mechanical modes. Such system paves the way for the realization of coherent THz to optical transducers and allows the realization of fundamental optomechanical systems in the THz frequency range.

***Corresponding authors: Allegra Calabrese and Yanko Todorov,** Laboratoire de Physique de l'Ecole Normale Supérieure, ENS, Paris Sciences et Lettres, CNRS, Université de Paris, 24 rue Lhomond, 75005 Paris, France, e-mail: allegra.calabrese@ens.fr (A. Calabrese); yanko.todorov@ens.fr (Y. Todorov).
https://orcid.org/0000-0002-2359-1611 (Y. Todorov)
Djamal Gacemi, Mathieu Jeannin, Angela Vasanelli and Carlo Sirtori: Laboratoire de Physique de l'Ecole Normale Supérieure, ENS, Paris Sciences et Lettres, CNRS, Université de Paris, 24 rue Lhomond, 75005 Paris, France
Stéphan Suffit: Laboratoire Matériaux et Phénomènes Quantiques, CNRS UMR 7162, Université de Paris, 75013 Paris, France.
https://orcid.org/0000-0002-7979-5138

Keywords: optomechanics; MEMS; Coulomb force; metamaterials; THz radiation.

1 Introduction

The interaction of the electromagnetic field with nano-scale mechanical resonators has gained considerable interest in recent decades [1–3]. Devices that realize such interaction are either optomechanical or electromechanical. In the first type, photons are trapped in an optical microcavity with at least one movable reflective boundary [4]. In the second type, the interaction is mediated through the electric field generated in the capacitive part of an inductor-capacitor resonant circuit [5]. In both cases, progressive miniaturization of mechanical oscillators has allowed increasing the sensitivity to the electromagnetic field [3, 6], enabling applications for infrared and THz detection [7, 8], chemical and biological sensing [9, 10], and optical and microwave signal processing [11, 12]. This increase in sensitivity has also allowed fundamental studies such as the exploration of the quantum regime of mechanical motion [13, 14] and the ultra-strong light-mechanical coupling regime [15]. Among other applications, electromechanical devices are particularly attractive for noise-free band-to-band converters in quantum communication systems, potentially able to transfer quantum states from superconducting qubits to optical fiber links [16–19]. In the present work, we demonstrate an electromagnetic THz meta-atom where a nano-mechanical element is reversibly driven by the Coulomb force of a THz electric field, even at room temperature. This structure, realizing the fundamental optomechanical Hamiltonian [1] in the THz, could become a key component in THz to near infrared (NIR), and possibly GHz to THz qubit converters [20].

The fundamental optomechanical interaction is described as the direct momentum and energy transfer between photons and the mechanical oscillator (radiation pressure) [21, 22], while in an electromechanical device the interaction is driven by Coulomb forces [23]. However, since the vast majority of devices are realized on solid-state

platforms, dissipative photo-thermal forces have strong and even dominant contribution to the overall mechanical response [13]. For this mechanism, the electromagnetic field produces a temperature rise in the material that leads to thermally induced mechanical stress. A main difference between optical/Coulomb and photothermal forces is that the latter are fundamentally retarded [13], with a time constant τ corresponding to heat diffusion along the mechanical element, while radiation pressure and Coulomb force act instantaneously on the mechanical motion. Photo-thermal forces can be exploited to realize very sensitive light detectors [7, 24] as well as for self-oscillation ("lasing") of mechanical resonators [25, 26]; however, they are unwanted for applications that require coherent transfer of information.

In the THz meta-atom described in this work, the fundamental electromagnetic resonance of the meta-atom is designed to generate a strongly localized electric field that pulls a metallic micro-beam (Figure 1). Photothermal effects arise due to heat induced by the absorbed THz radiation in the substrate supporting our devices. By analyzing the phase shift of mechanical oscillations with respect to the overall driving force, we are able to make a clear distinction between photothermal and Coulomb force and quantify the magnitude of the latter. This analysis has been detailed for the fundamental mechanical modes of the beam, where Coulomb and photothermal effects are on the same order of magnitude. We also show that the Coulomb contribution becomes dominant to the overall driving force (up to 94%) for the high-order modes of the beam, where photothermal effects become too slow with respect to the mechanical oscillation period.

2 Methods

2.1 Devices and fabrication procedure

Figure 1A presents the THz meta-atom. Its mechanical part consists of an all metallic doubly-clamped

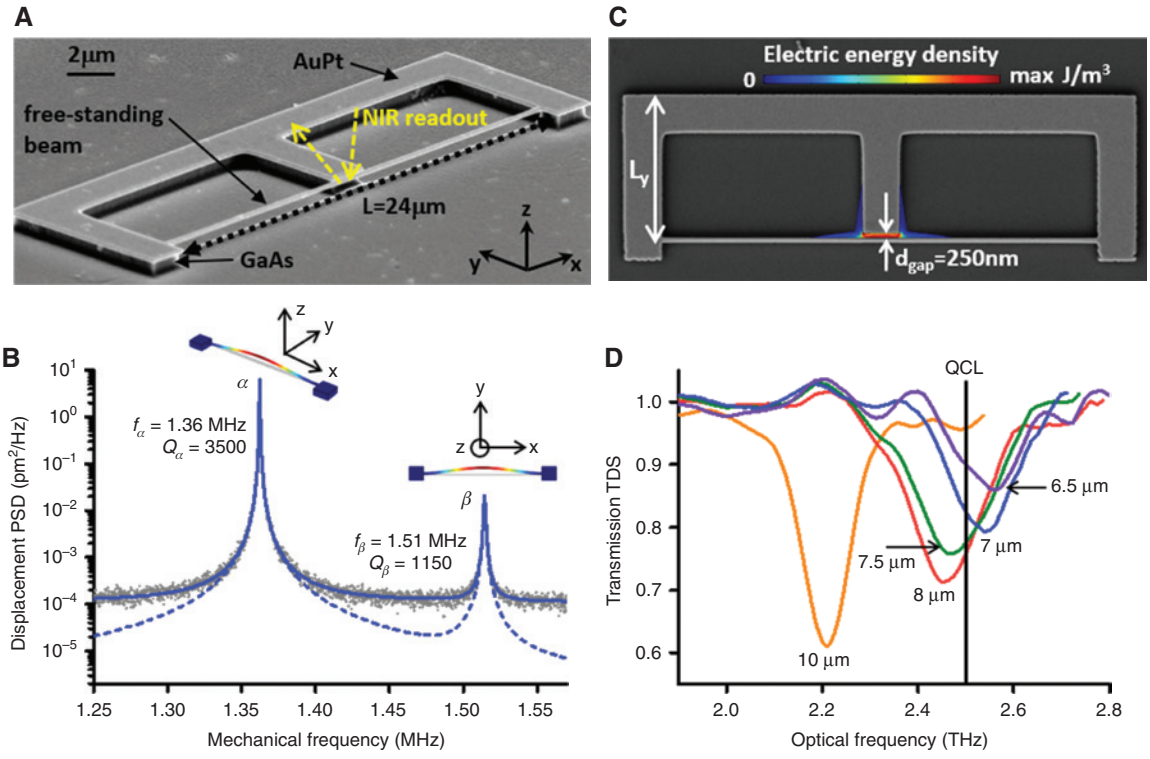

Figure 1: THz optomechanical meta-atom.
(A) Scanning electron micrograph of the double-split-ring resonator (DSR). (B) Measured thermo-mechanical (Brownian) noise power spectral density (PSD) of the beam showing the resonances that correspond to first-order flexural modes (dotted curve). The cartoons are finite element method (FEM) simulations of the modes. The blue dashed curve is a model based on Ref. [1]; the blue solid line takes into account the noise floor of the spectrum analyzer (see Supplementary Material). (C) Top-view scanning electron micrograph image of the device. Superposed is a FEM simulation of the electric energy density distribution at resonance. (D) THz time domain spectroscopy transmission spectra of 1.5×1.5 mm² arrays of identical devices. Each spectrum is identified by the value of the length L_y defined in panel C. The straight black line shows the emission frequency of our THz QCL source.

beam, in order to avoid the photothermal bilayer effect [27], which was dominant in devices developed in an earlier work [7]. The beam is combined with a double-loop split ring (DSR), which has an improved optical quality factor thanks to a reduced radiation loss [28]. The THz meta-atom was fabricated through standard clean-room processing, by depositing a metal pattern onto a semi-insulating GaAs substrate. After dry etching with inductively coupled plasma, the all-metal doubly-clamped beam is liberated through sulfuric acid etching of the underlying GaAs. In the final device, the beam has length $L = 24$ μm, width $w = 250$ nm and thickness $t = 155$ nm (where 5 nm is a Pt adhesion layer and the rest is Au). The beam stands at a vertical distance $h = 600$ nm from the substrate.

2.2 Mechanical properties

The mechanical modes of the system are probed optically, by shining a $\lambda = 910$ nm laser on the mechanical beam and detecting the reflected light on a split photodiode unit connected to a spectrum analyzer (SA). As the experiment is conducted at room temperature, clear peaks appear on the SA in correspondence of the beam mechanical modes, signatures of the thermomechanical noise (Brownian motion) [29]. The noise spectrum is shown in Figure 1B (dotted curve). It reveals the fundamental out-of-plane (α) and in-plane (β) modes, at frequencies $f_\alpha = 1.36$ MHz, $f_\beta = 1.51$ MHz, respectively, and quality factors $Q_\alpha = 3500$ and $Q_\beta = 1150$. To reduce viscous damping, measurements are performed in a vacuum chamber operated at a pressure around 10^{-1} mbar. Oscillation frequencies are calculated using Euler-Bernoulli theory [30, 31], with the addition of a tensile stress [32] with a typical value of 30 MPa. The latter is probably due to stress relaxation after etching of the GaAs supporting pillars. The Brownian motion spectrum is simulated using the expression from reference [1] for the thermal noise power spectral density (PSD) of a one-dimensional mechanical resonator, at room temperature, with a Lorentzian contribution for each mechanical resonance (dashed curve). The overall calculated PSD shown as a solid curve in Figure 1B includes the noise floor of the SA. The comparison between the simulated and measured PSD allows us to calibrate the mechanical readout of our system and provides the absolute value of the mechanical displacements. The different amplitudes of the α and β peaks are due to different detection sensitivities for out-of-plane and in-plane displacements [7] (see Supplementary Material).

2.3 Optical properties

Figure 1C shows a scanning electron micrograph of the device superposed with a finite element method simulation of electric energy density of the fundamental mode. This figure shows a strong electric energy build-up in the 250-nm wide gap. This part of the resonator acts as a capacitor, where charges of opposite signs are induced on both sides of the gap. Further analysis detailed in the Supplementary Material shows that the electric energy in this region is a fraction ($\eta = 1/10$) of the total electric energy of the resonance. This is an indication that the electromagnetic resonance is dominated by propagation effects corresponding to surface waves that run along the inductive loops [33]. The resonance corresponds to a standing wave pattern which creates an electric field maximum in the capacitive part. The resonant frequency can then be modeled as $f_{\mathrm{THz}} = c/(2n_{\mathrm{eff}} p)$, where c is the speed of light, n_{eff} is an effective index and $p = 2 \times (L/2 + L_y)$ is the perimeter of one loop of the DSR, with L_y indicated in Figure 1C. The frequency f_{THz} can therefore be adjusted solely through the length L_y while keeping the length L of the mechanical oscillator identical. Figure 1D shows measured transmission spectra of devices with variable values of L_y. The spectra were obtained using THz time domain spectroscopy on 1.5×1.5 mm^2 arrays of identical devices. For these experiments, the THz pulses are impinging on the arrays from the GaAs substrate through a Si hyperhemispherical lens (see Supplementary Material). The observed resonance dips are well fitted by Lorentzian lineshapes, with central frequencies and quality factors listed in Table 1. From these data we extract an average value of $n_{\mathrm{eff}} = 1.55$. This value applies to all resonators with a maximum error of approximately 2% on the resonance frequency (Table 1), confirming the standing wave model of the DSR resonance. It has also been confirmed by numerical modeling of the resonances that provide a value $n_{\mathrm{eff}} = 1.6$ in a frequency range between 1.6 THz and 3 THz (see Supplementary Material).

Table 1: Measured central frequency and quality factor and estimated central frequency for the THz time domain spectroscopy transmission spectra of Figure 1D.

L_y (μm)	f_{THz} (THz)	Q_{THz}	f_{THz} (THz) ($n_{\mathrm{eff}} = 1.55$)
10	2.21	23	2.19
8	2.46	16	2.41
7.5	2.47	15	2.48
7	2.54	20	2.54
6.5	2.55	22	2.61

3 Results and discussion

3.1 Mechanical response to THz radiation

The light-mechanical interaction is induced by shining on our devices a THz beam generated by a 2.5-THz quantum cascade laser (QCL) [34]. The beam impinges on the devices through the GaAs substrate and is focused by a hyperhemispherical Si lens, which is the same configuration used to obtain the transmission spectra in Figure 1D. The optical intensity of the QCL is modulated from 20 kHz to 6 MHz in order to explore the mechanical response of the system around the lowest order flexural modes. The mechanical output is detected by replacing the SA with a fast lock-in amplifier locked to the modulation frequency of the QCL. This set-up allows recording both amplitude and phase of the mechanical response induced by THz radiation. The 2.5-THz QCL emission line is also indicated in Figure 1D.

As discussed in the Supplementary Material, the QCL-induced photothermal force arises from the heating of the sample substrate and has a typical time constant $\tau = 0.7$ μs as estimated both from simulation and experiments. This force acts on both α- and β-resonances and is completely independent on the DSR resonance. Instead, the QCL-induced Coulomb force depends on the resonance of our meta-atoms, it acts instantaneously on the beam and it only drives the horizontal β-resonance. These three properties allow extracting the contribution of the Coulomb force from the overall mechanical response. Using these considerations, the complex forced mechanical displacement can be written as follows [13]:

$$u(f) = \frac{1}{1+i2\pi f\tau} \times \left(\frac{f_\alpha^2/Q_\alpha}{f_\alpha^2 - f^2 + if f_\alpha/Q_\alpha} + A_T \frac{f_\beta^2/Q_\beta}{f_\beta^2 - f^2 + if f_\beta/Q_\beta} \right) + A_C \frac{f_\beta^2/Q_\beta}{f_\beta^2 - f^2 + if f_\beta/Q_\beta} \quad (1)$$

Here, the maximum displacement of the α-resonance has been set to 1, while the constants A_T and A_C represent respectively the amplitude of the thermal and Coulomb contribution to the β-mode displacement. The retardation of the photothermal contribution is taken into account through the factor $(1+2\pi i\tau f)^{-1}$, which depends solely on the heat diffusion time τ. In order to disentangle the different contributions from Eq. (1), we need to study both the amplitude and the phase of the QCL-induced displacement as a function of the modulation frequency f. In our analysis we compare two structures: $L_y = 10$ μm, for which the DSR is out of resonance from the QCL emission (see Figure 1D), and $L_y = 8$ μm, which is nearly resonant. The corresponding amplitude and phase scans are shown respectively in Figure 2A and B ($L_y = 10$ μm) and Figure 2C and D ($L_y = 8$ μm). All measurements were taken with an incident modulated THz power of 1.36 mW.

The data for the $L_y = 10$ μm structure (Figure 2A and B, gray dots) are well reproduced assuming a purely thermal driving force for both modes [$A_C = 0$ in Eq. (1)]. The amplitude and phase (red solid lines) are well accounted for through Eq. (1) using the parameter values $\tau = 0.7$ μs, $f_\alpha = 1.049$ MHz, $Q_\alpha = 3300$, $f_\beta = 1.193$ MHz, $Q_\beta = 850$ and $A_T = 0.015$. The behavior of the phase corresponds to what is expected for two classical harmonic oscillators: for $f < f_\alpha$ both oscillators are in phase with the drive, while for $f > f_\beta$ they both have opposite phase. For $f_\alpha < f < f_\beta$ the β mode is in phase with the drive while the α mode has opposite phase, such that the total amplitude goes to zero at 1.17 MHz.

The data from Figure 2C and D (gray dots) are fairly different from those in panels A and B. Indeed, now the Coulomb force is important because the DSR mode is resonant with the QCL emission frequency. Very good fits for both amplitude and phase are obtained using the parameters $A_T = 0.058$ and $A_C = -0.0023$ (blue solid line). The other parameters are $\tau = 0.7$ μs, $f_\alpha = 1.358$ MHz, $Q_\alpha = 3500$, $f_\beta = 1.510$ MHz, $Q_\beta = 1150$. To understand the influence of the different contributions, we also compare the data with fits of Eq. (1) for two different cases: (i) purely thermal effects ($A_C = 0$, red dashed line) and (ii) purely instantaneous in-plane force ($A_T = 0$, green dotted line). In each case, the other parameter A_T or A_C is adjusted so as to obtain the best possible fit on the measured motion amplitude. Case (i) (red dashed curve) with $A_T = 0.072$ yields symmetric phase feature around the β-resonance, and predicts a zero amplitude at 1.48 MHz, which is not observed in the experiment. Case (ii) (green dotted line) with $A_C = -0.012$ predicts a strongly asymmetric dispersive-type behavior of the phase. This behavior can be explained by the absence of the retardation factor $(1+2\pi i\tau f)^{-1}$ for the Coulomb force. In the range of the β-resonance, we have $2\pi\tau f_\beta = 6.64$, and therefore the retardation factor $(1+2\pi i\tau f)^{-1} \sim -i0.15$ provides a quadrature phase difference between the Coulomb and the thermal force driving the α-resonance. The i-factor swaps the real and imaginary part of the mechanical response, leading to the dispersive-like behavior of the phase that arises from the real part.

When both Coulomb and thermal effects are taken into account, the Coulomb contribution introduces appreciable asymmetry in the phase feature around the β-resonance, in sharp difference with the symmetric feature that is expected with thermal force only. The absolute value of the thermal effect is $A_T' = A_T/[1+(2\pi f_\beta\tau)^2]^{1/2} = 0.0087$. Since the total displacement at $f = f_\beta$ can be expressed as

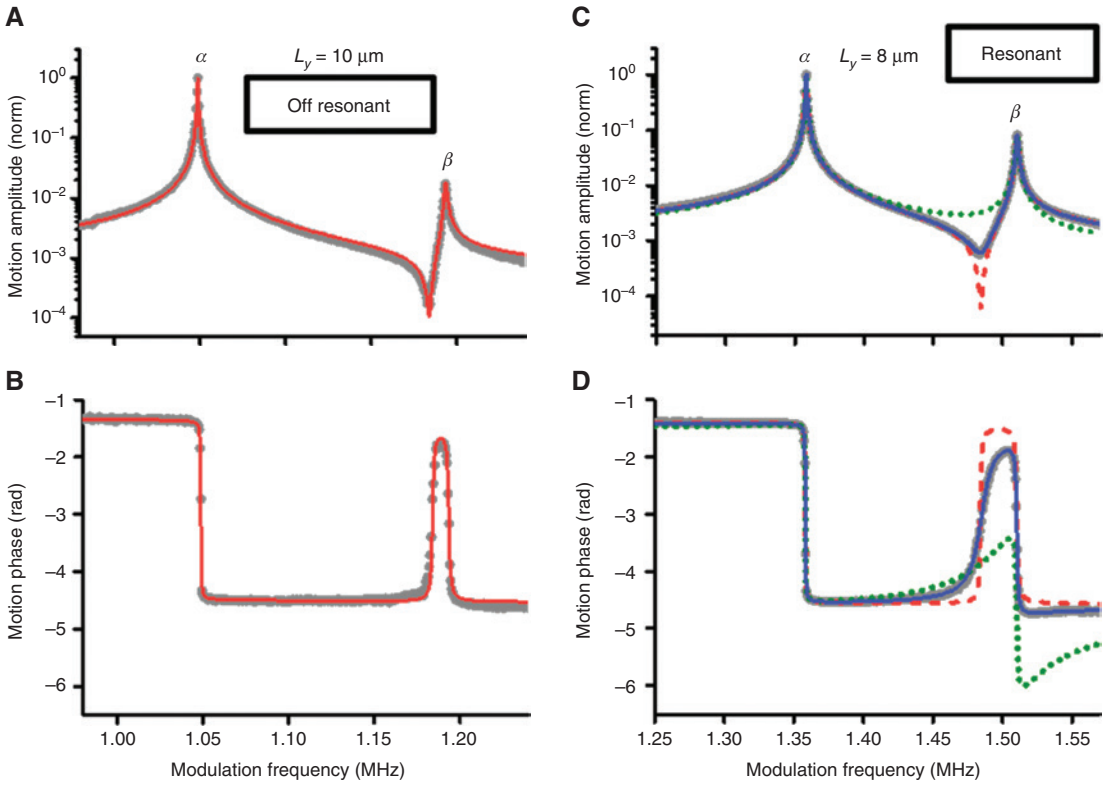

Figure 2: Mechanical response for structures with various detuning from the incident THz beam.
(A and B) Amplitude and phase of forced mechanical oscillations of the mechanical beam, for a non-resonant DSR having $L_y = 10$ μm. Gray dots: scan data. Red solid lines: amplitude and phase calculated from the model of Eq. (1) with $A_C = 0$, corresponding to two thermally driven modes. (C and D) Amplitude and phase of forced mechanical oscillations of the beam, for a resonant DSR having $L_y = 8$ μm. Gray dots: scan data. Red dashed lines: amplitude and phase calculated from the model of Eq. (1) with $A_C = 0$, corresponding to two thermally driven modes. Green dotted lines: amplitude and phase calculated from Eq. (1) with $A_T = 0$, corresponding to a thermally driven α mode and a Coulomb-driven β mode. Blue solid lines: amplitudes and phase calculated from Eq. (1), corresponding to a thermally driven α mode and a β mode which is 26% Coulomb driven.

$u(f_\beta) = (-A_C + iA'_T)$, we deduce that the in-plane driving force is $A_C / |u(f_\beta)| = A_C / [A_C^2 + A_T'^2]^{1/2} = 26\%$ electromechanical. Note that the coefficients A_T and A_C have opposite signs: this signifies that the thermal and Coulomb force push the cantilever into opposite directions. This is expected, as the Coulomb force is attractive, pulling the beam toward the gap, whereas the thermal expansion pushes it outward.

3.2 Magnitude of the Coulomb force

Having determined the fraction of the Coulomb force in the overall driving force, we can now determine its absolute value. To this end, as shown in Figure 3, we compare the spectra recorded on the SA around the β-resonance in the presence of QCL radiation (red curve) and with the QCL blocked (blue curve). The absolute values on the vertical axis are obtained by setting the maximum of the Brownian noise spectral density at the value [1] $S_{yy}(f_\beta) = 2k_B T Q_\beta / [m_{\text{eff}} \omega_\beta^3] = 2.16$ pm²/Hz (here $m_{\text{eff}} = 6.9$ pg is the beam effective mass and $\omega_\beta = 2\pi f_\beta$). The QCL modulated at f_β produces a delta-like spectral density with an integral of 4.2×10^5 pm². The total THz-induced displacement is then $u(f_\beta) = 650$ pm (these measurements were taken on a different $L_y = 8$ μm structure which showed 29% Coulomb effect). Therefore the Coulomb-driven displacement is $y_{\text{Coul}} = 187$ pm, taking into account the phase quadrature between the thermal and Coulomb forces. The absolute value of the Coulomb force is then $F_{\text{Coul}} = m_{\text{eff}} \omega_\beta^2 y_{\text{Coul}} / Q_\beta = 0.09$ pN. The QCL induces a frequency red-shift of the mechanical resonance owing to thermally induced stress [35].

The magnitude of the Coulomb force can be modeled by the following equation:

$$F_{\text{Coul}} = -\frac{W_{e\text{THz}}}{d_{\text{gap}}^{\text{eff}}} \tag{2}$$

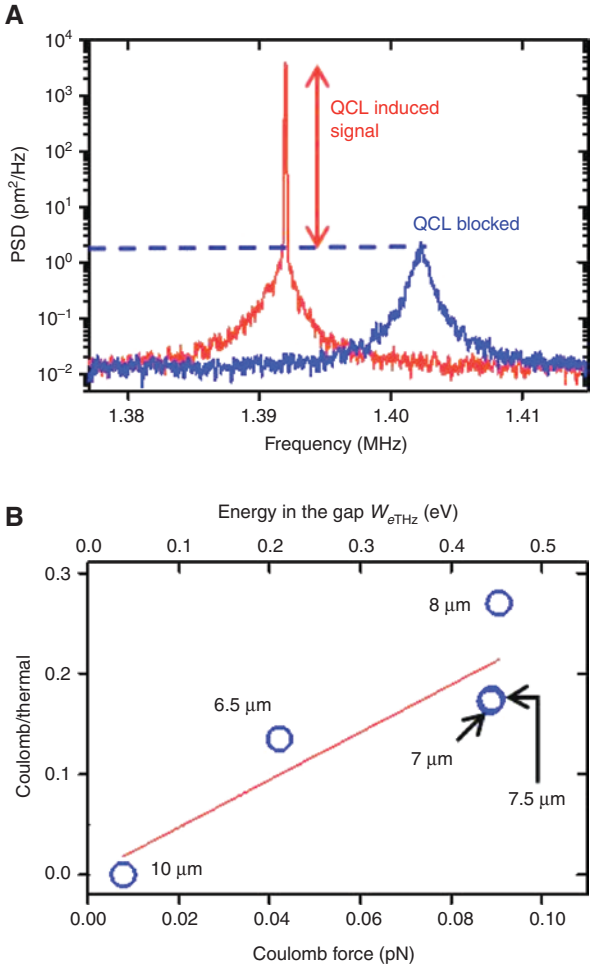

Figure 3: Estimate of the Coulomb force for the first-order mechanical mode.
(A) SA spectra recorded with (red curve) and without (blue curve) THz radiation on the sample, with the QCL modulated at the frequency of the mechanical resonance f_β. The dashed line corresponds to the peak noise spectral density $S_{yy}(f_\beta)$ of the Brownian motion. The 10 kHz redshift of f_β with the QCL on is due to heating effect. (B) Ratio of the Coulomb to thermal effect on the β mode as a function of the Coulomb force F_{Coul}, for structures identified by the value of the length L_y (see Figure 1C and D). The top *x*-axis reports the values of the electric energy in the gap W_{eTHz}. Blue dots are data and the red line is a linear fit.

Here W_{eTHz} is the electric energy around the gap between the cantilever and the rest of the DSR (see Figure 1C), and d_{gap}^{eff} is an effective length which is expressed as $1/d_{gap}^{eff} = d\ln W_{eTHz}/dy|_{y=d_{gap}}$. The energy W_{eTHz} is related to the power P_{in} coupled into the resonator through the formula $W_{eTHz} = (0.5\,\eta\, Q_{THz}/\omega_{THz})\, P_{in}$, where $\omega_{THz} = 2\pi f_{THz}$ and $\eta \sim 1/10$ represents the fraction of the total electric energy of the resonator which is stored in the gap. To determine d_{gap}^{eff} we have simulated the distribution of electric energy W_{eTHz} in the gap as a function of the plate separation *y* (see Supplementary Material). The results of the simulation indicate a value of $d_{gap}^{eff} = 885$ nm, which is larger than the real gap of 250 nm because of fringing field effects [7]. With this value we obtain a Coulomb force of 60 fN for $P_{in} = 1$ µW of total power dropped in the resonator. From the value of the Coulomb force that we have estimated from our measurements ($F_{Coul} = 0.09$ pN), we deduce that the power dropped in the resonator is approximately 1.3 µW. This value is approximately six times smaller than the value expected assuming that the QCL emits a Gaussian beam (Supplementary Material) [36]. This difference can be ascribed to the imperfect alignment between the Si lens and the single meta-atom structure, as well as scattering on different interfaces. Figure 3B summarizes our estimates of the fraction $R = A_C/\{A_T/[1+(2\pi f_\beta\,\tau)^2]^{1/2}\}$ between the Coulomb and the thermal contribution to the β-resonance as a function of the Coulomb force F_{Coul} for all measured structures. The trend is linear as expected; the scattering of the experimental points can be ascribed to the various uncertainties commented above. These results show that the Coulomb force is at maximum 1/3 of the total mechanical force for the first-order in-plane mechanical resonance. An estimate of the electric energy W_{eTHz} coupled in the gap following Eq. (2) is also provided in the upper horizontal axis.

3.3 Coulomb effect on higher-order mechanical modes

To further reduce the photothermal contribution, we exploit the intrinsic advantage of the Coulomb force with respect to thermal forces: the fact that it acts instantaneously on the system. As the amplitude of thermal effects scales as $1/\sqrt{1+(2\pi f\tau)^2}$, they will be suppressed at higher frequency, while the Coulomb force will remain constant. We therefore expect that the electromechanical effect is much stronger on higher-order flexural modes. Since, according to our design, the Coulomb force is applied only to the middle point of the beam, we expect that second-order modes, which have a node in that position, have a purely thermal response, even for the structures resonant with the QCL. This was indeed observed for the DSR with $L_y = 8$ µm, as reported in the Supplementary Material. In Figure 4, we report the results for the third-order modes of the $L_y = 8$ µm structure, which maximize the mechanical displacement in the center of the beam. Analysis of the Brownian motion of the third-order modes provides their frequencies $f_{\alpha 3} = 4.54$ MHz, $f_{\beta 3} = 5.51$ MHz and quality factors $Q_{\alpha 3} = 2400$ and $Q_{\beta 3} = 2500$. Amplitude and phase data of forced mechanical motion are reported in Figure 4A and B, respectively (gray dots). As for our previous analysis, we provide fits of the data based on Eq. (1). Now, the

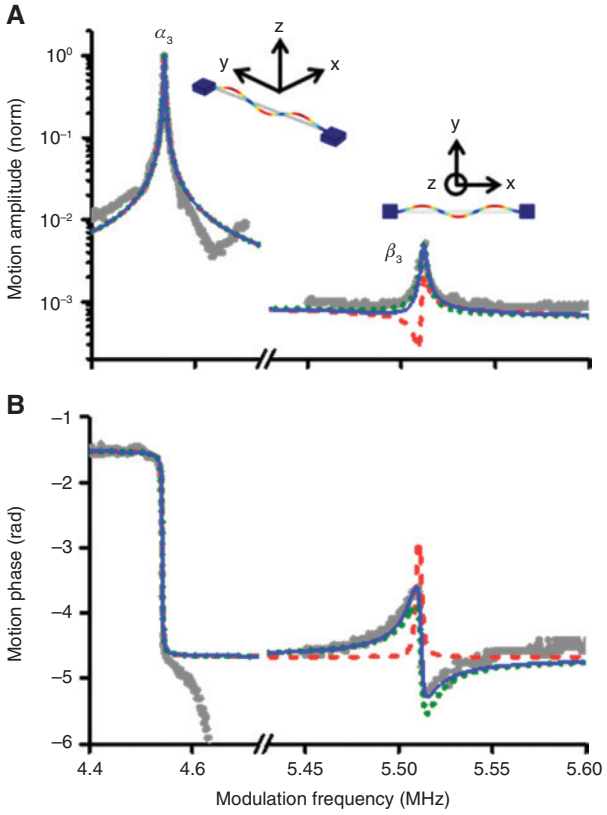

Figure 4: Mechanical response for third-order flexural modes. Cartoons are FEM simulations of the mode shapes. (A and B) Amplitude and phase of forced mechanical oscillations. Gray dots: experimental data. Scans on the two modes were taken separately, setting the phase of the lock-in to zero before each scan. The measurement was taken under an incident modulated THz power of 1.75 mW. Red dashed lines: amplitude and phase calculated from the model of Eq. (1) with $A_c = 0$, corresponding to two thermally driven modes. Green dotted lines: amplitudes and phase calculated from the model of Eq. (1) with $A_T = 0$, corresponding to a thermally driven α_3 mode and a Coulomb-driven β_3 mode. Blue solid lines: amplitudes and phase calculated from the model of Eq. (1), corresponding to a thermally driven α_3 mode and a β_3 mode which is 94% Coulomb driven.

hypothesis of purely thermal forces misses completely the experimental data (red dashed line). We observe instead a dispersive-like profile of the phase of the β_3 mode, almost as expected for a purely Coulomb-driven resonance (green dotted curve). A more accurate fit is obtained by assuming 94% Coulomb projection on the overall driving force. This reduced value of thermal effects is well accounted for by the retardation factor $1/\sqrt{1+(2\pi f\tau)^2}$.

3.4 Final remarks

Considering our system from the point of view of the fundamental electromechanical Hamiltonian, we estimate the vacuum optomechanical coupling as $g_{om} = \eta\omega_{THz} y_{ZPF}/d_{eff} = 53$ kHz [1] with $y_{ZPF} = 30$ fm the zero-point amplitude of the beam modes considered here. In our experiments, typically 6×10^3 phonons are excited, which leads to a mechanically induced frequency shift of the THz meta-atom in the order of 0.3 GHz. This value is small compared to the THz DSR mode linewidth (~100 GHz). Therefore, while our device converts efficiently the THz radiation into a mechanical movement, the back-action of the mechanical movement on the THz frequency is negligible. However, improvements to boost the value of g_{om} are possible. For instance, three-dimensional THz meta-atom architectures allow for almost perfect confinement of the electric energy, $\eta \sim 1$, in the capacitive parts [37]. While for THz meta-atoms typical quality factors are bound on the order of $Q_{THz} \sim 100$, an interesting alternative would be to use the mechanical displacement to control the mode coupling in Fano-type systems [8].

4 Conclusions

In conclusion, we have studied the dissipative and reactive forces that couple mechanical movement to THz radiation in specially designed THz meta-atoms. We have shown that the effect of the Coulomb force, which is excited resonantly with the external radiation, can be extracted from the non-resonant thermal background effects. Furthermore, these forces become dominant for high-order mechanical modes, with an oscillation period that is much faster than thermal diffusion time in the system. Such conservative forces can be exploited for band-to-band conversion between THz and other frequency domains, and even for quantum coherent information transfer at low temperature, where photothermal forces and thermal noise are canceled. Indeed, the THz band (0.1–10 THz) is now considered as the next frontier for telecommunication links [38]. Advanced applications such as quantum secure communications have already been envisioned [20]. Therefore, band-to-band efficient transducers from the THz range to NIR domain could be of paramount interest for future quantum communication systems. For instance, the mechanical element can be shared with the capacitive part of a GHz [5] or radio frequency [39] circuit, or with the reflective part of an optical cavity [40]. Finally, combining our device with frequency phase-locked loop (PLL) technique [41], we can use the instantaneous Coulomb force for THz detector applications [42], where the detection bandwidth is limited only by the PLL circuit.

Acknowledgments: This work was supported by the French National Research Agency under the contracts ANR-16-CE24-0020 and ANR-18-CE24-0025, Funder Id: http://dx.doi.org/10.13039/501100001665.

References

[1] Aspelmeyer M, Kippenberg T-J, Marquardt F. Cavity optomechanics. Rev Mod Phys 2014;86:1391–452.
[2] Kippenber T-J, Vahala K-J. Cavity optomechanics: back-action at the mesoscale. Science 2008;321:1172–6.
[3] Ekinci K-L, Roukes M-L. Nanoelectromechanical systems. Rev Sci Instrum 2005;76:061101.
[4] Favero I, Karrai K. Optomechanics of deformable optical cavities. Nat Photon 2009;3:201–5.
[5] Teufel J-D, Li D, Allman M-S, et al. Circuit cavity electromechanics in the strong-coupling regime. Nature 2011;471:204–8.
[6] Sapmaz S, Blanter Y-M, Gurevich L, van der Zant H-S-J. Carbon nanotubes as nanoelectromechanical systems. Phys Rev B 2003;67:235414.
[7] Belacel C, Todorov Y, Barbieri S, Gacemi D, Favero I, Sirtori C. Optomechanical terahertz detection with single meta-atom resonator. Nat Commun 2017;8:1578.
[8] Manjappa M, Pitchappa P, Singh N, et al. Reconfigurable MEMS Fano metasurfaces with multiple-input–output states for logic operations at terahertz frequencies. Nat Commun 2018;9:4056.
[9] Jimzewski J-K, Gerber C, Meyer E, Schlittler R-R. Observation of a chemical reaction using a micromechanical sensor. Chem Phys Lett 1994;217:589–94.
[10] Gil-Santos E, Baker C, Nguyen D-T. High-frequency nano-optomechanical disk resonators in liquids. Nat Nanotech 2015;10:810–6.
[11] Alves F, Pimental L, Grbovic D, Karunasiri G. MEMS terahertz-to-infrared band converter using frequency selective planar metamaterial. Sci Rep 2018;8:12466.
[12] Tsvirkun V, Surrente A, Raineri F, et al. Integrated III-V photonic crystal – Si waveguide platform with tailored optomechanical coupling. Sci Rep 2015;5:16526.
[13] Metzger C, Favero I, Ortlieb A, Karrai K. Optical self cooling of a deformable Fabry-Perot cavity in the classical limit. Phys Rev B 2008;78:035309.
[14] Teufel J-D, Donner T, Li D. Sideband cooling of micromechanical motion to the quantum ground state. Nature 2011;475:359–63.
[15] Gil-Santos E, Labousse M, Baker C, et al. Light-mediated cascaded locking of multiple nano-optomechanical oscillators. Phys Rev Lett 2017;118:063605.
[16] Ockeloen-Korppi C-F, Damskägg E, Pirkkalainen J-M, et al. Stabilized entanglement of massive mechanical oscillators. Nature 2018;556:478–82.
[17] Marinković I, Wallucks A, Riedinger R, Hong S, Aspelmeier M, Gröblacher S. Optomechanical Bell test. Phys Rev Lett 2018;121:220404.
[18] Riedinger R, Wallucks A, Marinković I, et al. Remote quantum entanglement between two micromechanical oscillators. Nature 2018;556:473–7.
[19] Regal C-A, Lehnert K-W. From cavity electromechanics to cavity optomechanics. J Phys Conf Ser 2011;264:012025.
[20] Ottaviani C, Woolley M-J, Erementchouk M, et al. Terahertz quantum cryptography. 2018; arXiv:1805.03514.
[21] Law C-K. Interaction between a moving mirror and radiation pressure: a Hamiltonian formulation. Phys Rev A 1995;51:2537–41.
[22] Cripe J, Aggarwal N, Singh R, et al. Radiation-pressure-mediated control of an optomechanical cavity. Phys Rev A 2018;97:013827.
[23] Roy Chowdhury D, Xu N, Zhang W, Singh R. Resonance tuning due to Coulomb interaction in strong near-field coupled metamaterials. J Appl Phys 2015;118:023104.
[24] Zhang Y, Watanabe Y, Hosono S, Nagai N, Hirakawa K. Room temperature, very sensitive thermometer using a doubly clamped microelectromechanical beam resonator for bolometer applications. Appl Phys Lett 2016;108:163503.
[25] Barton R-A, Storch I-R, Adiga V-P, et al. Photothermal self-oscillation and laser cooling of graphene optomechanical systems. Nano Lett 2012;12:4681–6.
[26] De Alba R, Abhilash T-S, Rand R-H, Craighead H-G, Parpia J-M. Low-power photothermal self-oscillation of bimetallic nanowires. Nano Lett 2017;17:3995–4002.
[27] Barnes J-R, Stephenson R-J, Woodburn C-N, et al. A femtojoule calorimeter using micromechanical sensors. Rev Sci Instrum 1994;65:3793–8.
[28] Al-Naib I, Yang Y, Dignam M-M, Zhang W, Singh R. Ultra-high Q even eigenmode resonance in terahertz metamaterials. Appl Phys Lett 2015;106:011102.
[29] Cleland A-N, Roukes M-L. Noise processes in nanomechanical resonators. J Appl Phys 2002;92:2758–69.
[30] Cleland A-N. Foundations of nanomechanics. Los Angeles, CA, Springer, 2002.
[31] Timoshenko S. Vibration problems in engineering. New York, NY, D. Van Nostrand Company, Inc., 1937.
[32] Unterreithmeier Q-P, Faust T, Kotthaus J-P. Damping of nanomechanical resonators. Phys Rev Lett 2010;105:027205.
[33] Zhou J, Koschny T, Soukoulis C-M. Magnetic and electric excitations in split ring resonators. Opt Expr 2007;15:17881–90.
[34] Barbieri S, Alton J, Beere H-E, Fowler J, Linfield E-H, Ritchie D-A. 2.9THz quantum cascade lasers operating up to 70K in continuous wave. Appl Phys Lett 2004;85:1674–6.
[35] Zhang X-C, Myers E-B, Sader J-E, Roukes M-L. Nanomechanical torsional resonators for frequency-shift infrared thermal sensing. Nano Lett 2013;13:1528–34.
[36] Richter H, Rothbart N, Hübers H-W. Characterizing the beam properties of terahertz quantum-cascade lasers. J Infr Mill Ter Wav 2014;35:686–98.
[37] Jeannin M, Mariotti Nesurini G, Suffit S, et al. Ultrastrong light–matter coupling in deeply subwavelength THz LC resonators. ACS Photon 2019;6:1207–15.
[38] Akyildiz I-F, Jornet J-M, Han C. Terahertz band: next frontier for wireless communications. Phys Commun 2014;12:16–32.
[39] Andrews R-W, Peterson R-W, Purdy T-P, et al. Bidirectional and efficient conversion between microwave and optical light. Nat Phys 2014;10:321–6.
[40] Stapfner S, Zadkov V-N, Durt T, et al. Cavity nano-optomechanics: a nanomechanical system in a high finesse optical cavity. Brussels, Belgium, SPIE Photonics Europe, 2010.

[41] Albrecht T-R, Grütter P, Horne D, Rugar D. Frequency modulation detection using high-Q cantilevers for enhanced force microscope sensitivity. J Appl Phys 1991;69:668–73.
[42] Zhang Y, Hosono S, Nagai N, Hirakawa K. Novel bolometric THz detection by MEMS resonators. 2018 43rd International Conference on Infrared, Millimeter, and Terahertz Waves (IRMMW-THz), Nagoya, Japan, 2018.

Supplementary Material: The online version of this article offers supplementary material (https://doi.org/10.1515/nanoph-2019-0314).